Int J Adv Manuf Technol (2017) 88:2651–2660
DOI 10.1007/s00170-016-8959-8

ORIGINAL ARTICLE

Friction stir welding of AA5052: the effects of SiC nano-particles addition

Mohsen Bodaghi[1] · **Kamran Dehghani**[1]

Received: 13 October 2015 / Accepted: 20 May 2016 / Published online: 6 June 2016

Abstract In the present work, the AA5052 aluminum sheets were joined by friction stir welding (FSW) technique. In order to refine the microstructure of stir zone (SZ) and to prevent the grain growth of heat-affected zone (HAZ), the SiC nano-particles were added to the weld nugget. To obtain the optimum condition for FSW, three rotational speeds (800, 1000, and 1250 rpm) and three traveling speeds (30, 50, and 80 mm/min) were applied. Microstructural evolutions were characterized using optical and scanning electron microscopes. Besides, the mechanical properties (tensile strength, hardness, and wear test) of weldment were also studied. The results showed that adding the SiC nano-particles led to the significant grain refining of the welds. However, the improper SiC powder distribution during one pass of FSW resulted in the premature fracture of workpiece. The specimens joined at the rotational speed of 1000 rpm and welding speeds of 50 and 80 mm/min exhibited the highest ultimate tensile strength.

Keywords FSW · AA5052 · Nano-composite · Mechanical performance · Microstructural characteristics

1 Introduction

The major demands in transportation industry such as automotive and aerospace are a reduction in weight and fuel consumption. To meet these requirements, the light metals such as aluminum alloys are the best candidates [1, 2]. Among aluminum alloys, the AA5052 is widely used in building, construction, automotive, aircraft, marine, etc. because of its excellent corrosion resistance, weldability, high fatigue strength, and moderate strength [3, 4].

However, the major concern regarding the aluminum alloys is their poor weldability when the conventional fusion welding is used. That is because there are many shortcomings during the fusion welding of aluminum alloys, e.g., gas and shrinkage porosities, solidification cracks, slag inclusions, etc. Thus, the conventional welding techniques are not suitable for joining the aluminum alloys [5, 6]. On the other hand, the most promising method for welding of aluminum alloys is friction stir welding (FSW), which was developed as a solid-state welding technology [7]. This process has been successfully used for welding of similar and dissimilar aluminum alloys [8–11]. Contrary to the fusion welding processes, there is no melt during FSW. Consequently, this process overcomes the shortcomings of conventional fusion welding [6].

During the FSW, the heat is generated by friction between tool and base metal. The applied pressure leads to severe plastic deformation as well. The generated heat is strongly influenced by welding parameters and can be controlled by traveling and rotation speeds. When other factors are kept constant, higher heat input is obtained by increasing the rotational speed and/or by decreasing the traveling speed. Higher heat input leads to better plastic flow of material and the wider nugget whereas the lower heat input will result in the narrower nugget [7, 11].

Many efforts are made to fabricate the metal matrix composites by friction stir processing (FSP) as well [12–14]. In all of these works, the researchers tried to produce a composite layer on a metal surface while no joining takes place during FSP. It was found that the number of FSP passes had significant effect on the particles distribution such that the further the

✉ Kamran Dehghani
dehghani@aut.ac.ir

[1] Mining and Metallurgical Engineering Department, Amirkabir University of Technology (AUT), P.O. Box: 15875-4413, Tehran, Iran

FSP passes offered better particle distribution [15, 16]. The effects of rotating and travel speeds on powder distribution and mechanical properties of composites, fabricated by FSP, were studied by many researchers. Asadi et al. [17] produced AZ91/SiC composite by FSP. They reported that an increase in the rotating and travailing speeds led to a decrease in the grain size.

Sun et al. [18] used SiC powders during the FSW of copper sheets. They incorporated nano-particles in the weld line and investigate the effect of these particles on the microstructure and mechanical properties of welds. It was shown that SiC particles were aggregated in the first pass but their distribution became more uniform after employing the second pass. Bahrami et al. [6] used SiC nano-particles during the FSW of AA7075-O sheets. They reported that adding the nano-particles in stir zone led to enhancement of mechanical properties of joints. They reported the presence of defects and banded structure consisting of particle-rich and particle-free regions in some of specimens as a result of SiC addition. Abbasi et al. [19] used SiC nano-particles during the FSW of AZ31 magnesium alloy and investigated the effect of nano-particles on microstructure and mechanical properties. Their results showed that the added SiC particles were distributed throughout the nugget zone. Consequently, metal matrix composite was successfully fabricated by employing proper rotation and traverse speeds. Abdolahzadeh et al. [20] investigated the effect of SiC nano-particles on the microstructure and mechanical properties of AZ31 alloy too. They observed onion ring structure containing SiC-rich and SiC-free regions in the SZ of welded specimens. They reported that by adding the SiC nano-particles, the grain size was reduced from 44 μm in base metal to 5 μm in the SZ.

The wear resistance of different materials and composites processed by the FSW and FSP has been studied by many researchers [21–24]. The metal matrix composites prepared in these works exhibited lower friction coefficient and better wear resistance compared to unprocessed specimens. Barmouz et al. [25] investigated the wear properties of Cu/SiC composite prepared by FSP. Their results showed that increasing the volume fraction of reinforced particles enhanced the wear resistance of composite layer. They also reported that the addition of nano-particles increased the wear resistance more significantly compared to micro-size SiC particles.

The aim of this study was to join the AA5052-O aluminum sheets as well as to fabricate the Al-SiC nano-composite simultaneously. The effect of SiC nano-particles on the mechanical properties and microstructural evolutions of weldments were also investigated.

2 Experimental procedure

The AA5052-O aluminum sheets with 4 mm in thickness were joined by FSW. Table 1 shows the composition of the studied alloy. In order to add the SiC nano-particles to the stir zone, a groove of 0.6 mm in width and 3.5 mm in depth was designed, Fig. 1. The SiC powders had the diameter in the range of 45 to 64 nm. To prevent scattering of particles during the FSW, the top of the groove was first covered using a tool that had a shoulder of 14 mm in diameter. The main welding tool had a concave shoulder with 14 mm in diameter. The threaded pin had the length and diameter of 3.7 and 4 mm, respectively (Fig. 2). The tools used in this study were made of H13 steel. The FSW was carried out at the rotating speeds of 800, 1000, and 1250 rpm and traveling speeds of 30, 50, and 80 mm/min. The tilt angle was 2.5°, whereas the plunge depth was 0.6 mm. The employed conditions and the codes of specimens are given in Table 2.

Table 1 Chemical compositions of used Al alloy (wt.%)

Element	Si	Fe	Mg	Mn	Cr	Cu	Al
Alloy AA5052-O	0.25	0.23	2.55	0.07	0.15	0.03	Balance

To study the microstructural evolution, the specimens were etched for 20 s using modified Poulton solution. The etching solution composed of 50 mL of Poulton reagent (12 mL HCl + 6 ml HNO_3 + 1 mL HF (48 %) + 1 mL H_2O), 25 mL HNO_3, and 40 mL of a solution consisting of 3 g chromic acid per 10 mL water. Afterward, the microstructural changes were characterized using optical and scanning electron microscopy (SEM). The SEM technique was also used to investigate the fracture surface of specimens.

In order to study the mechanical properties of welds, the strength, micro-hardness, and wear resistance of joints were investigated. Prior to the preparation of tensile specimens, top surfaces of joints were machined to remove the marks left by the shoulder. The sub-sized tensile specimens were prepared according to ASTM E8M-04. Tensile test was carried out at a cross-head speed of 1 mm/min.

Micro-hardness test was carried out on the center line of the SZ employing a 100 g load for 15 s.

The wear test was performed on the top surface of joints using the pin on disk method; the test was carried out under the normal load of 15 N. The rotating and sliding speeds were 144 rpm and 0.09 mm/s, respectively.

3 Results and discussion

3.1 Microstructural observation

Figure 3 shows the typical macrostructures of AA5052 after the FSW. As mentioned previously, the size of the nugget can be affected by heat input. Figure 3b is related to specimen that has experienced lower heat input compared to Fig. 3a due to higher traveling speed. As can be seen, the lower heat input in

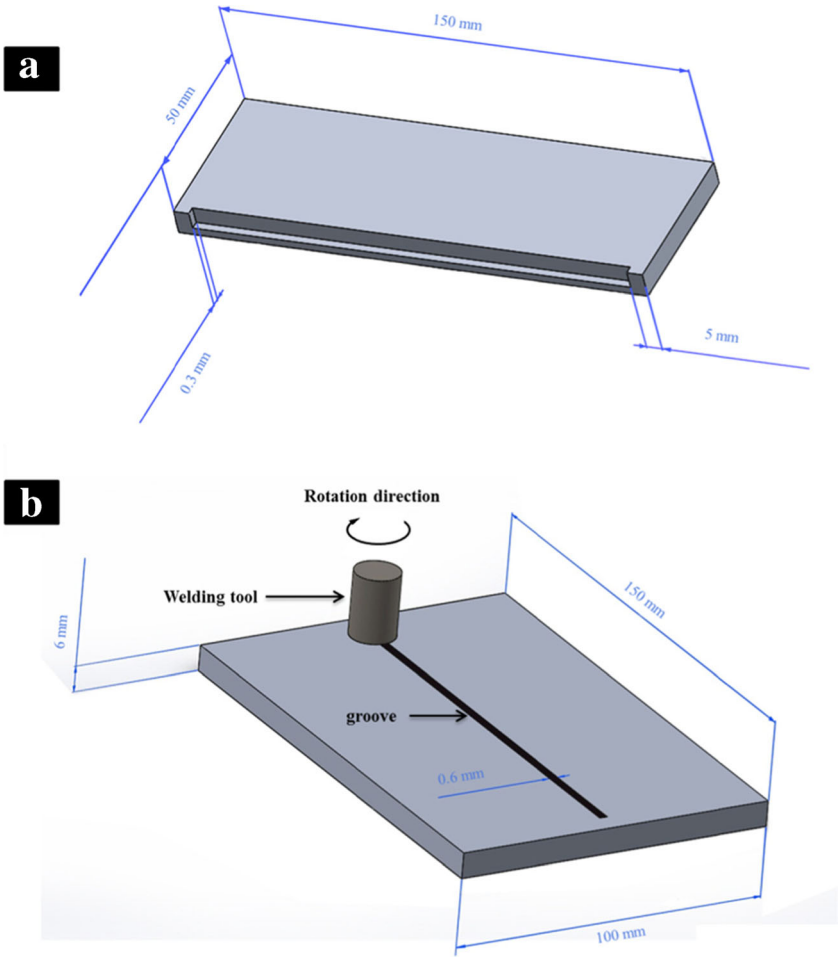

Fig. 1 Dimension of **a** machined adjoining side of sheets and **b** prepared groove after matching (dimensions are in millimeter)

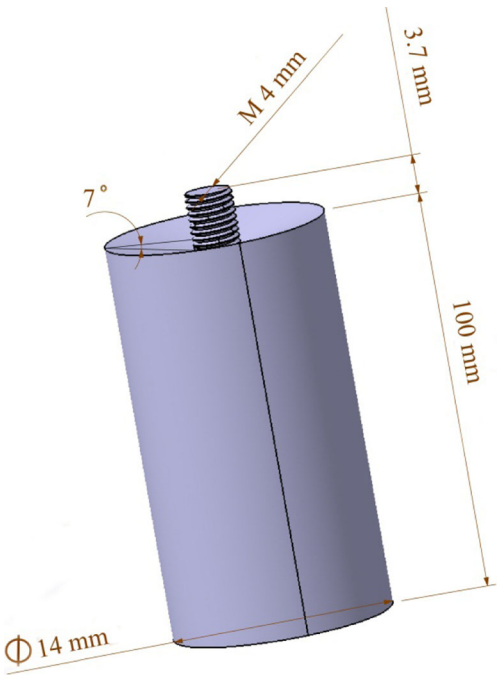

Fig. 2 Schematic of FSW tool

this specimen has led to the smaller nugget. Figure 3b shows a wider nugget comparing to two previous specimens that led to higher rotating speed and consequently higher heat generation. This effect was also seen in other specimens.

On the other hand, the level of generated heat has pronounced effect on weld soundness. As it can be seen in Fig. 3b, the big holes are formed in the nugget zone due to insufficient heat generation in the joining process resulting in the improper material flow. However, by increasing the rotating speed to 1000 rpm, the sound welds were produced, i.e., specimen 1000-50 shown in Fig. 3c. In case of specimen 1250-80, the zigzag-type path was observed in the stir zone (SZ). In this specimen, some kind of powder agglomeration was observed. Increasing the welding speed and/or decreasing the rotating speed led to insufficient heat input and consequently to low material flow. In such a case, the zigzag mark or tunnel defect can occur in the SZ. Besides, the improper material flow can result in localized accumulation of particles and in the zigzag line [26]. Thus, in the mentioned specimen, the high welding speed is likely responsible for the observed defect.

However, the intact welds were obtained at the traveling speed of 50 mm/min for all studied rotating speeds. Therefore,

Table 2 Specimens code and process conditions

Specimen number	Specimen code[a]	Rotation speed (rpm)	Traveling speed	Condition
1	800-30	800	30	With powder
2	800-50	800	30	With powder
3	800-80	800	30	With powder
4	1000-30	1000	50	With powder
5	1000-50	1000	50	With powder
6	1000-80	1000	50	With powder
7	1250-30	1250	80	With powder
8	1250-50	1250	80	With powder
9	1250-80	1250	80	With powder
10	1000-50-n	1000	50	Without powder

Welding condition: tilt angle, 2.5°; plunge depth, 0.6 mm; rotation direction, clockwise

[a] The first number indicates the rotation speed and the second indicates the traveling speed

it can be concluded that 50 mm/min is the optimum travel speed in the current work.

Figure 4 illustrates the initial microstructure of AA5052 having the average grain size of 36 μm. During FSW, there are generally four zones: base metal (BM), heat-affected zone (HAZ), thermo-mechanically affected zone (TMAZ), and stir zone (SZ) [8, 27, 28]. For the specimen 1000-50, these zones are shown in Fig. 5. Referring to this figure, the grain size of

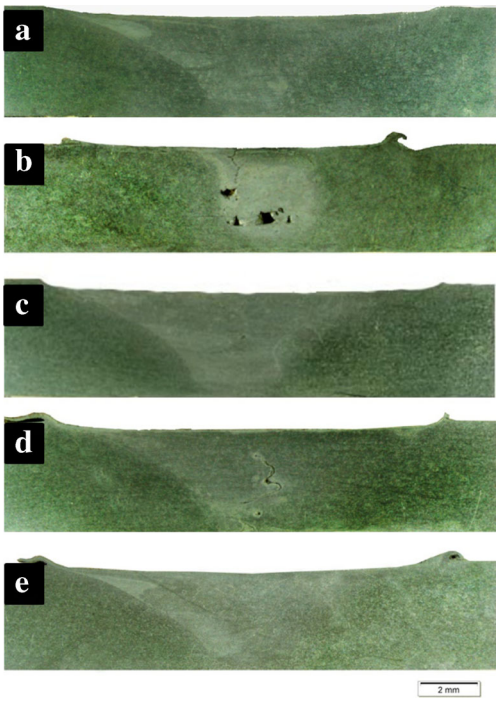

Fig. 3 Imperfections in cross section profile of specimens **a** 800-50, **b** 800-80, **c** 1000-50, **d** 1250-80, and **e** 1000-50-n

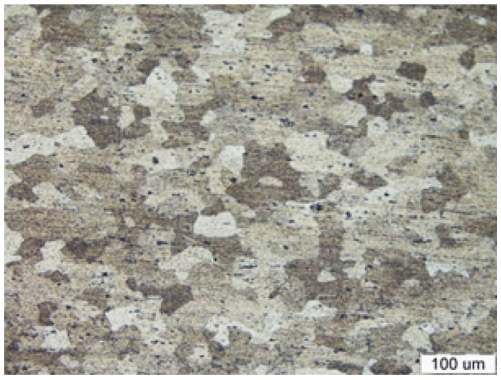

Fig. 4 Microstructure and grain size of base metal before welding process

SZ is considerably smaller than that of the base metal. This is attributed to the severe plastic deformation and continues dynamic recrystallization occurring in the SZ [7, 27].

The presence of reinforced particles is another factor that influences the grain size of SZ. The added particles act as barriers against grain boundary motion and prevent the grain growth via Zener effect [5, 29]. According to Zener pinning effect, the driving force for grain boundary migration would be counteracted by the pinning pressure exerted by reinforcement particles. Consequently, normal grain growth would be inhibited and the average grain size could not exceed a critical maximum grain radius (R_C) given by the equation $R_C = 4r/3f$, where r and f are the radius and volume fraction of reinforcements, respectively [30]. Thus, the nano-particle incorporation in the weld line results in finer grains in the nugget.

However, the distribution of particles is a major concern regarding the fabrication of reinforced composites. The difference in the distribution of SiC nano-powders is obvious in case of 1000-80 specimen, Fig. 6. According to this figure, there is a difference in the grain size between the particle-rich and particle-free regions. For instance, the mean grain size of SZ in the particle-rich regions (5 μm) is obviously smaller than that of the particle-free regions (12 μm). This confirms the effect of SiC nano-powders on the

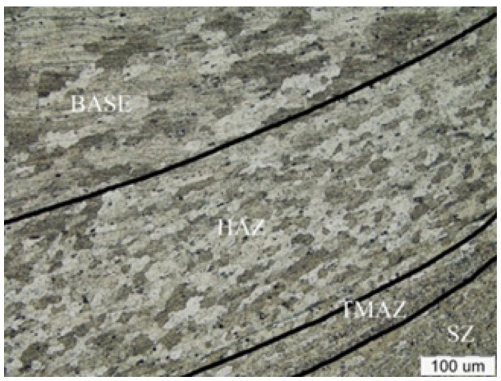

Fig. 5 Different zones in joint area of specimen 1000-50-n

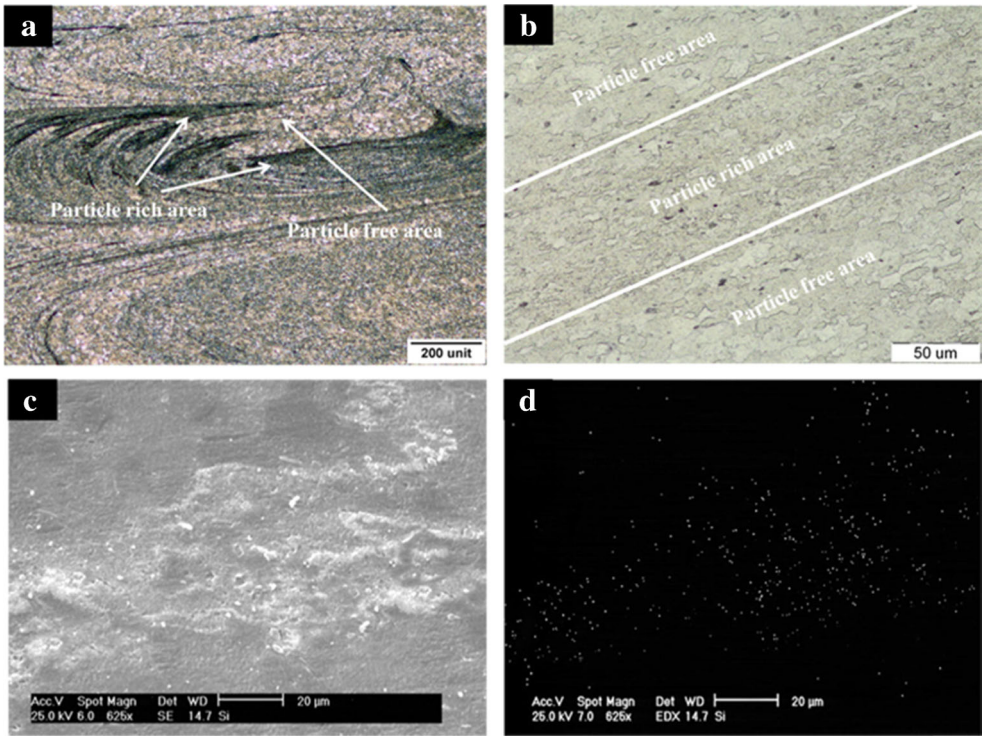

Fig. 6 Banded structure in SZ of specimen 1000-80: **a** distribution of SiC particles in SZ and formation of particle-free and particle-rich regions, **b** grain size difference between these regions, **c** SEM micrograph of particle-rich and particle-free regions, and **d** Si WDS image of (**c**)

refining of microstructure. In this regard, the effect of nano-powder addition is obvious by comparing the microstructures of 1000-50 and 1000-50-n specimens. It can be seen that the specimen 1000-50 has a mean grain size considerably smaller (about 70 %) than that of the specimen 1000-50-n which had no SiC nano-powders.

The grain sizes related to different zones of all specimens are summarized in Table 3. All the weld nuggets show the formation of fine recrystallized equiaxed grains because of applied severe plastic deformation and the occurrence of dynamic recrystallization. On the other hand, as noted earlier, the SiC nano-particles exhibit significant impeding effect on the grain-boundary movement, which in turn results in the grain-size refinement of SZ.

Referring to Table 3, an increase in the rotating speed has led to larger grain size in the weld nugget. At a constant traverse speed, as the rotating speed increases, the generated heat increases and consequently the nugget grains will grow [2, 26]. Cavaliere et al. [31] also reported that the grain size in the weld nugget of AA6056 joints was increased with increasing the rotating speed from 500 to 800 rpm. On the other hand, the grain size was decreased by increasing the traveling speed. This is due to lower level of heat input provided at higher traveling speeds [7]. As FSW resembles the hot severe plastic deformation (SPD), the generated heat as well as the applied strain rate

Table 3 the grain sizes related to different zones

Specimen code	SZ grain size (μm)	TMAZ grain width (μm)	HAZ grain size (μm)	BM grain size (μm)
800-30	14	17	38	36
800-50	11	20	35	36
800-80	5	22	36	36
1000-30	9	17	40	36
1000-50	5	17	37	36
1000-80	7	18	35	36
1250-30	11	16	39	36
1250-50	9.5	16	36	36
1250-80	6.5	17	37	36
1000-50-n	12	18	42	36

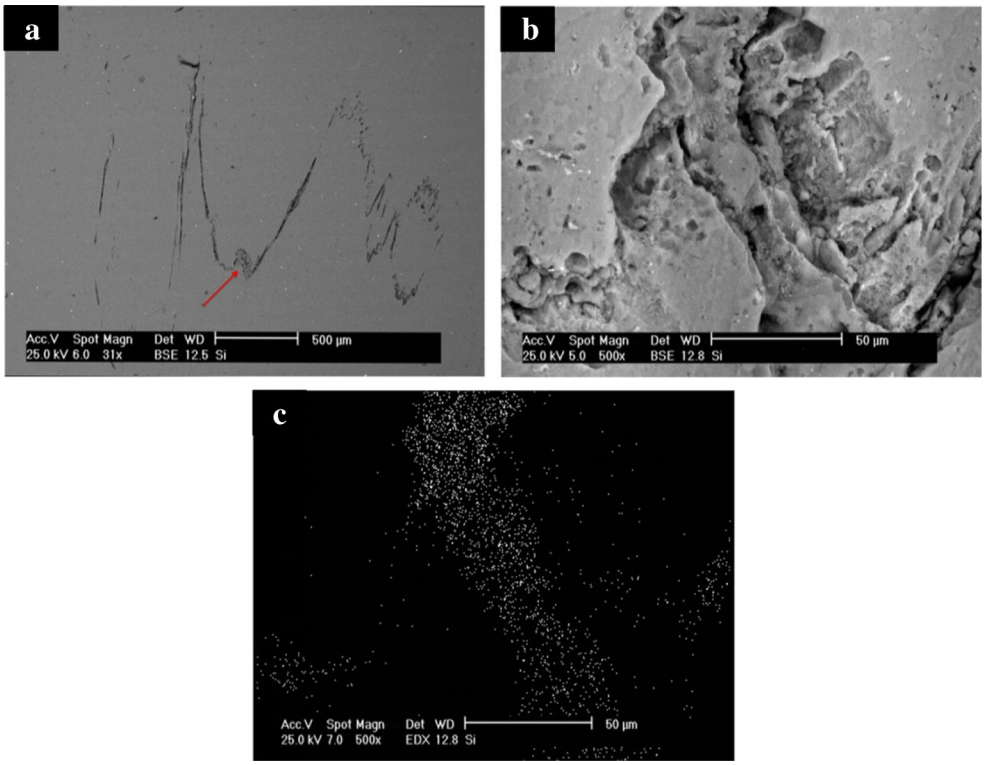

Fig. 7 SEM image of SZ of specimen 1000-50, **a** powder accumulation in zigzag line, **b** high magnification of highlighted area, and **c** Si WDS image of (**b**)

have significant effect on the grain refining so that the size of dynamically recrystallized grains decreases with decreasing the temperature or increasing the strain rate [2].

Figure 7 depicts the SEM images taken from agglomerated SiC particles in the specimen 1000-50. In Fig. 7a, the SiC nano-particles are accumulated in a zigzag-type line. Figure 7b presents the higher magnification of the marked region in Fig. 7a. The defects such as cracks/microvoids can be formed adjacent to these agglomerated particles due to the poor adhesion between the particles and matrix. Figure 7c illustrates the Si map taken from the area of Fig. 7b. This figure conforms that the SiC nano-particles are agglomerated in this region.

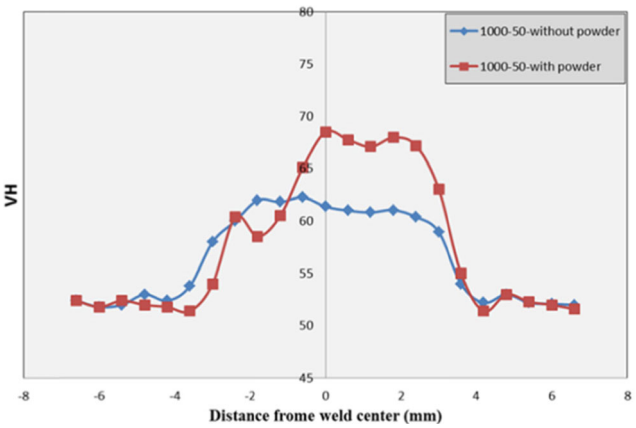

Fig. 8 Variation of micro-hardness in the centerline of weld nugget for specimen 1000-50 with and without nano-particles

3.2 Microhardness

SiC particles exhibit pronounced effect on microhardness of nugget. In fact, if they are agglomerated they can act as preferred nucleation sites via particle stimulate nucleation (PSN) mechanism for the formation of new grains during dynamic recrystallization. This results in extensive small grains. After the recrystallization and in the grain growth stage, the individual SiC particles suppress grain coarsening by impeding the boundaries and resulting in finer grains, i.e., Zener effect. On the other hand, these ceramic particles have high hardness themselves [14, 30] which exhibit strong resistance to dislocation motion. Therefore, the produced nanocomposite exhibited high levels of hardness and strength.

The micro-hardness profiles taken from the weld nugget of specimen 1000-50 with and without the addition of SiC nano-particles are presented in Fig. 8. Obviously, the micro-hardness amount increased with adding nano-particles. Referring to Table 3, it is clear that the specimen produced using nano-particles has much smaller grains compared to without particle one. These finer grains are responsible to higher hardness.

Figure 8 also shows that when the powders were added, the hardness in advancing side (AS) was higher than that of retreating side (RS). However, in case of FSW without

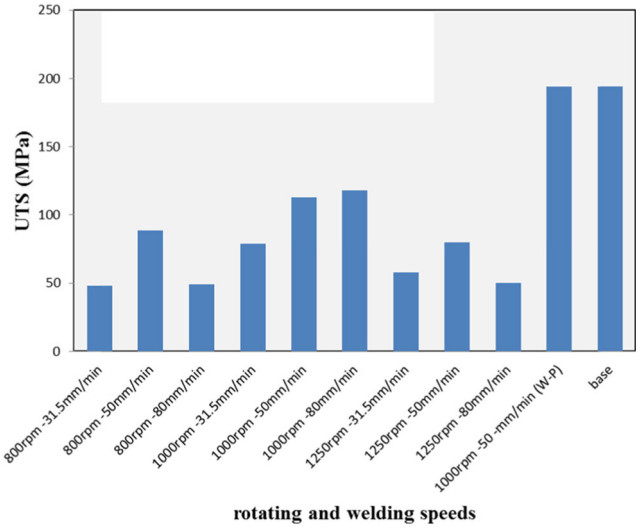

Fig. 9 UTS values at all welds in comparison with the base metal

powders, the hardness profile shows the same trend for both AS and RS. In other words, the hardness profile regarding the specimen without nano-particles shows a more uniform hardness in the SZ. This difference in the behavior of two sides implies that the difference between the retreating side and advancing side are enhanced due to the addition of nano-particles.

3.3 Tensile test

Ultimate tensile strength (UTS) of parent metal and welds are shown in Fig. 9. According to this diagram, the specimens welded at the rotating speed of 1000 rpm and traveling speeds of 50 and 80 mm/min have maximum UTS among all specimens. This result shows that SiC particles are distributed more uniform under these conditions.

Figure 10 shows the fracture appearance and failure location of the tensile specimens of 1000-50 and 1000-50-w. As it can be seen in Fig. 10a, for the 1000-50 specimen, fractures occurred at the advancing side with no plastic deformation. This is in good agreement with the results reported by Sun and Fuji [18]. They noted that after the FSW of copper, the failure occurred in the area having severely agglomerated SiC particles. Bahrami et al. [6] also reported the similar results in the FSW of AA7075 alloy containing nano-powders. Referring to Fig. 10, the accumulated powders (dark region) in the fracture zone of 1000-50 specimen are clearly visible in this figure. In case of 1000-50-n specimen, Fig. 10b, the failure took place in the base metal and far from the nugget, showing necking and noticeable ductility. As for the specimens welded using incorporated SiC particles, the failure occurred in the regions of accumulated powders, a logical correlation between the strength and microstructure of specimens cannot be established.

Figure 11 presents the SEM images of fracture surface regarding the 1000-50 and 1000-50-n specimens. As illustrated in the Fig. 11a, the SiC particles are severely accumulated and in turn failure can take place around this area. It is most likely that the agglomerated powders acted as the crack-nucleation sites and this is the reason for the low UTS of this sample. As noted previously concerning Fig. 10, for specimen 1000-50-w, the failure occurred after necking in the base metal. The fracture appearance of this specimen indicates its ductile fracture, Fig. 11b. As a result, the agglomeration of SiC particles, caused by improper distribution of these particles due to one pass of FSW, is responsible for premature fracture and low strength of samples processed by only one pass of FSW.

The strengthening mechanism of FSW composite can be explained based on (i) Hall-Petch, (ii) Orowan strengthening, and (iii) dislocation strengthening. These are somehow discussed in the Sections 3.2 and 3.5. As mentioned there, the nano-particles can pin the grain boundaries and in turn prevent the grain growth. In such a case, the smaller grains led to higher strength and hardness according to Hall-Petch equation. As for the interaction of particles with dislocations, two cases can take place depending on the size of particles. If

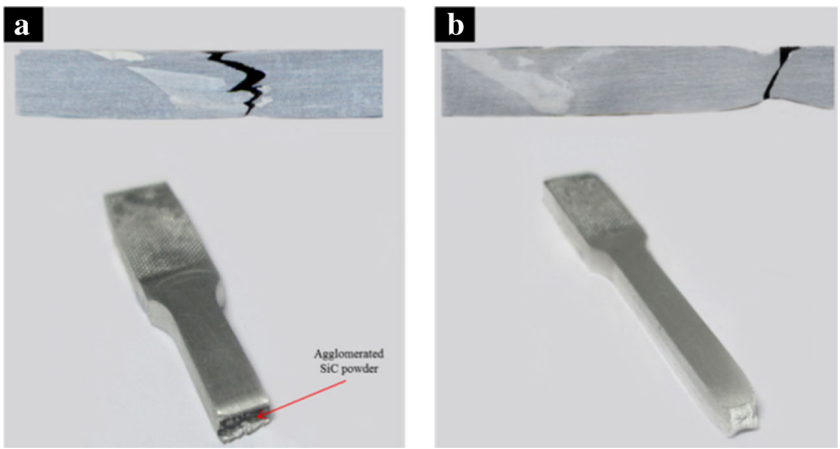

Fig. 10 Cross section and fracture location of tensile specimens after failure of **a** 1000-50 with powder and **b** 1000-50 without powder

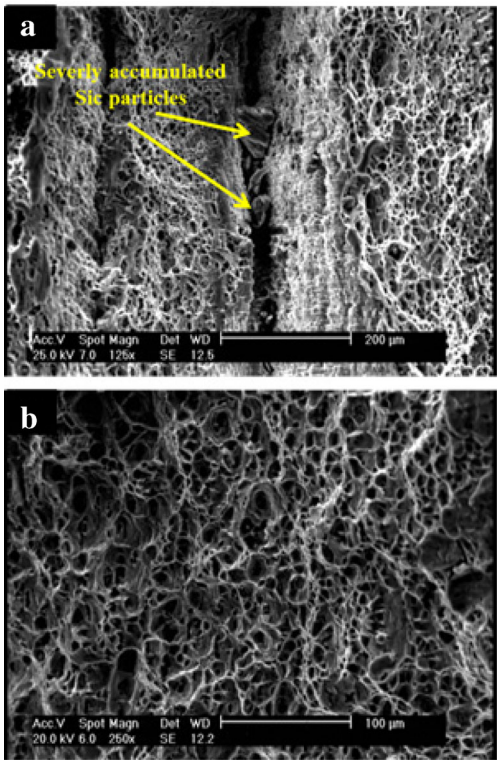

Fig. 11 Fracture micrographs of 1000-50 specimens **a** with nano-powder and **b** without nano-powder

the size of particles is small, the dislocation can cut the particles and then are piled up leading to strengthening. However, in case of large particles, the lopping occurs which again leads to strengthening the materials.

3.4 Wear test

The results of wear testing are presented in Fig. 12 and Table 4. These include the weight loss and the friction coefficients diagrams regarding the 1000-50 and 1000-50-n specimens compared to the parent metal. Referring to these results, in case of 1000-50-n specimen, the friction coefficient is greatly lower than that of the starting material (i.e., not subjected to FSW). This is most likely because of smaller grain size and higher hardness in the SZ of FSWed sample. As for the 1000-50 specimen, the friction coefficient is lower than that of the starting material but higher than that of the1000-50-n specimen. The addition of SiC particles led to a decrease in the friction coefficient provided that these particles uniformly distributed within the metal matrix. Thus, the decrease in friction coefficient can be enhanced by increasing the number of FSW passes [32]. That is because the improper distribution of particles results in the powder accumulation. In such a case, a poor adhesion between the particles and matrix will exist. Therefore, during the wear testing of this specimen, the lamination and separation of surface layer can take place rather than erosion that leads to higher weight loss compared to the starting material and 1000-50-n specimen. According to Fig. 12, the higher amplitude of friction profile of this specimen can be also as the result of improper distribution of SiC particles.

3.5 Strengthening mechanisms

In all strengthening mechanisms, the strength is enhanced by prohibiting the mobility of dislocations. In such cases, the reinforcements or second particles pin the grain boundaries or act as an obstacle for dislocation motion opposing the dislocation mobility resulting in an increase in material strength.

Grain boundary serves as a barrier to the movement of glide dislocations. According to Hall-Petch equation ($\sigma_{ys} = \sigma_i + k_y d^{-1/2}$), the yield strength of polycrystalline materials depends on the grain size. Thus, the finer the grain size, the higher the yield strength will be. A practical and useful approach to refine the gains is introducing the reinforce particles in the matrix. This is especially more beneficial in case of materials which suffer from the lack of second phases to pin

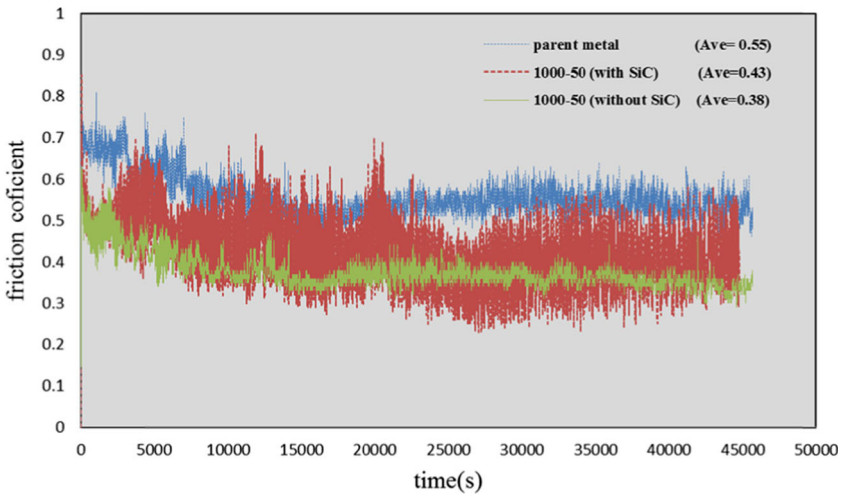

Fig. 12 Effect of one pass welding of specimen 1000-50 on friction coefficients

Table 4 Weight loss of the 1000-50 specimens and the base metal after wear test

	Weight loss (mg)
Parent metal	4.3
1000-50 (with SiC)	8.3
1000-50 (without SiC)	3.2

the boundaries or when the grain-boundary mobility is high due to the material characteristics.

When the dislocation mobility in a solid is restricted by the introduction of solute atoms, the resultant strengthening is called solid-solution strengthening. It is well known that any solute implies a stress/strain field due to the size difference with solvent atoms. This stress/strain is enhanced when the size of solutes are too large or too small in relation to the size of the host atom. A solute atom is said to be a point source of dilation. Consequently, the stress resulted from the interactions of dislocations and solute-atom fields can lead to extra strengthening. Such an interaction due to size difference is called the elastic misfit interaction or dilational misfit interaction. This interaction represents an energy barrier to dislocation motion.

Alloys can be also strengthened by addition of reinforcements/particles that obstruct dislocation motion. For example, by adding the SiC particles to aluminum alloys, the material receives attractive strength properties even up to its melting temperature. However, the increase in strength depends on the both volume fraction and inter-particle spacing. As for their size, the strengthening potential for dislocation looping around incoherent particles is normally less than that associated with particle cutting process. Thus, comparing to other methods, this kind of strengthening can be among the strongest hardening techniques. With respect to microstructure, the reinforced alloys are more stable than those hardened by precipitation, thereby making them more suitable for load bearing application at elevated temperatures.

The last type of strengthening is work hardening. In this regard, the enhanced strength can be attributed to the high dislocation density. However, in the presence of reinforcements/second particles, this effect is much more pronounced since there is another source for increasing the dislocation density as a result of the large difference in the formability and/or thermal expansion (about 10:1) of the metal matrix and the added ceramic particles. Accordingly, such mismatch/misfit strains can be relieved by the generation of new dislocations around these particles, leading to enhanced strengthening.

4 Conclusions

The effect of welding parameters and the addition of SiC nano-particles on the microstructure and mechanical properties of AA5052 alloy joined by FSW were investigated. The results can be summarized as follows:

1. The optimum rotating and traveling speeds were 1000 rpm and 50 mm/min, respectively.
2. The addition of SiC nano-particles exhibited pronounced effect on the grain refining of the nugget as the reinforcements act as preferred nucleation sites and also pin the grain boundaries, So that the mean grain size reduced from 36 μ in base metal to 5 μm in case of the 1000-50 specimen.
3. The specimen prepared using SiC nano-particles had lower UTS compared to the without powder specimen. The powder agglomeration in the SZ is responsible to this phenomenon.
4. The microhardness of the SZ of the specimen produced using nano-particles is considerably higher than that of the specimen without powder. This is as the result of the presence of hard ceramic particles (SiC) and also the role of these particles in reducing of the grain size via Zener effect and also impeding dislocation mobility.
5. Improper powder distribution in the SZ led to lower wear resistance and higher weight loss of specimens during wear test. This is due to particles accumulation and poor adhesion between the agglomerated particles and the matrix which leads to lamination and separation of surface layer.
6. One pass FSW resulted in the agglomeration of SiC nano-particles in the advancing side so that failure of tensile specimens occurred in this area.

Acknowledgments The authors acknowledge the financial support of Iran Nanotechnology Initiative Council. Also, they wish to express their grateful thanks to Dr. Masoud Alizadeh-sh for his constant help and encouragement.

References

1. Zhang Z et al (2011) Effect of welding parameters on microstructure and mechanical properties of friction stir spot welded 5052 aluminum alloy. Mater Des 4461–4470
2. Kwon YJ, Shim SB, Park DH (2009) Friction stir welding of 5052 aluminum alloy plates. Trans Nonferrous Met Soc China 23–27
3. Kaufman JG (2000) Introduction to aluminum alloys and tempers. ASM Int
4. (2004) ASM handbook 02
5. Dolatkhah A et al (2012) Investigating effects of process parameters on microstructural and mechanical properties of Al5052/SiC metal matrix composite fabricated via friction stir processing. Mater Des 458–464
6. Bahrami M, Dehghani K, Givi MKB (2013) A novel approach to develop aluminum matrix nano-composite employing friction stir welding technique. Mater Des 53:217–225
7. Mishra RS, Mahoney MW (2007) Friction stir welding and processing. ASM Int

8. Khaled T (2005) An outsider looks at friction stir welding. ANM-112N-05-06
9. Yazdanian S, Chen ZW, Littlefair G (2012) Effects of friction stir lap welding parameters on weld features on advancing side and fracture strength of AA6060-T5 welds. J Mater Sci 1251–1261
10. Sato YS, Urata M, Kokawa H (2002) Parameters controlling microstructure and hardness during friction-stir welding of precipitation-hardenable aluminum alloy 6063. Metall Mater Trans A 32
11. Shi L, Wu CS, Liu HJ (2015) The effect of the welding parameters and tool size on the thermal process and tool torque in reverse dual-rotation friction stir welding. Int J Mach Tools Manuf 91:1–11
12. Dadashpoura M et al (2016) Effect of process parameter on mechanical properties and fracture behavior of AZ91C/SiO2 composite fabricated by FSP. Mater Sci Eng A 655:379–387
13. Khodabakhshia F et al (2015) Hot deformation behavior of an aluminum-matrix hybrid nanocomposite fabricated by friction stir processing. Mater Sci Eng A 626:458–466
14. Navazani M, Dehghani K (2016) Fabrication of Mg-ZrO2 surface layer composites by friction stir processing. J Mater Process Technol 229:439–449
15. Sharifitabar M et al. (2011) Fabrication of 5052Al/Al2O3 nanoceramic particle reinforced composite via friction stir processing route. Mater Des 4164–4172
16. Yang M et al. (2010) Fabrication of AA6061/Al2O3 nano ceramic particle reinforced composite coating by using friction stir processing. 4431–4438
17. Asadi P, Faraji G, Besharati MK (2006) Producing of AZ91/SiC composite by friction stir processing (FSP). Int J Adv Manuf Technol 247–260
18. Sun YF Fujii H (2011) The effect of SiC particles on the microstructure and mechanical properties of friction stir welded pure copper joints. Mater Sci Eng A 5470–5475
19. Abbasi M et al (2015) The effect of SiC particle addition during FSW on microstructure and mechanical properties of AZ31 magnesium alloy. J Mater Eng Perform 24:5037–5045
20. Abdolahzadeh A et al (2014) Studying microstructure and mechanical properties of SiC-incorporated AZ31 joints fabricated through FSW: the effects of rotational and traveling speeds. Int J Manuf Technol 75:1189–1196
21. SATHISKUMAR R et al (2015) Evaluation of the microstructure and wear behaviour of AA6063-B4C/TiB2 mono and hybrid composite layers produced by friction stir processing. Trans Nonferrous Metals Soc China 25:95–102
22. Sudhakar I et al (2015) Enhancement of wear and ballistic resistance of armour grade AA7075 aluminium alloy using friction stir processing. Def Technol 11:10–17
23. Yuvaraj N, Aravindanb S, Vipin (2015) Fabrication of Al5083/B4C surface composite by friction stir processing and its tribological characterization. J Mater Res Technol 4:398–410
24. Narimani M, Lotfi B, Sadeghian Z (2016) Evaluation of the microstructure and wear behaviour of AA6063-B4C/TiB2 mono and hybrid composite layers produced by friction stir processing. Surf Coatings Technol 285:1–10
25. Barmouz M et al (2011) Investigation of mechanical properties of Cu/SiC composite fabricated by FSP: effect of SiC particles' size and volume fraction. Mater Sci Eng A528:1740–1749
26. Sharma C, Dwivedi DK, Kumar P (2012) Effect of welding parameters on microstructure and mechanical properties of friction stir welded joints of AA7039 aluminum alloy. Mater Des 379–390
27. Lohwasser D, Chen Z (2010) Friction stir welding from basics to applications. CRC
28. Singh G, Singh K, Singh J (2011) Effect of process parameters on microstructure and mechanical properties in friction stir welding of aluminum alloy. Trans Indian Inst Met 64:325–330
29. Arora HS, Singh H, Dhindaw BK (2012) Composite fabrication using friction stir processing—a review. Int J Adv Manuf Technol 1043–1055
30. Bahrami M, Nikoo MF, Givi MKB (2015) Microstructural and mechanical behaviors of nano-SiC-reinforced AA7075-O FSW joints prepared through two passes. Mater Sci Eng A 626:220–228
31. Cavaliere P et al. (2009) Effect of welding parameters on mechanical and microstructural properties of dissimilar AA6082–AA2024 joints produced by friction stir welding. Mater Des 609–616
32. Sarmadi H, Kokabi AH, Reihani SMS (2013) Friction and wear performance of copper–graphite surface composites fabricated by friction stir processing (FSP). Wear 304:1–12